KARYA ILHAM PUBLISHING
CONNECTING MINDS, BRIDGING IDEAS, INSPIRING READERS

Advances in Fluid, Heat and Materials Engineering

Journal homepage:
https://karyailham.com.my/index.php/afhme/index
ISSN: 3083-8134

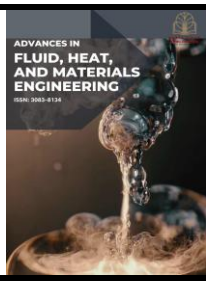

Simulation of Flow Pattern Around a Triangular Prism with Different Base Angles

Eng Shao Tang[1,*], Ahmad Alif Ashraf[1], Ahmad Danial[1], Ahmad Nadzim[1], Aiman Akmal[1]

[1] Faculty of Mechanical and Manufacturing Engineering, Universiti Tun Hussein Onn Malaysia, 86400 Parit Raja, Batu Pahat, Johor, Malaysia

ARTICLE INFO

Article history:
Received 13 January 2026
Received in revised form 21 February 2026
Accepted 5 March 2026
Available online 31 March 2026

Keywords:
Triangular prism; computational fluid dynamics; bluff body aerodynamics; wake topology; flow separation

ABSTRACT

The study of external fluid dynamics over bluff bodies is a cornerstone of aerodynamic and civil engineering, fundamental to designing structures that can withstand significant wind loads. Unlike streamlined shapes, bluff bodies like triangular prisms induce strong flow separation, creating complex wake regions that directly influence structural stability. However, the specific impact of the prism's base angle on the intensity of this separation and the resulting drag forces remains a critical parameter that requires detailed quantification. The primary purpose of this research is to investigate the external flow dynamics around triangular prisms with distinct base angles of 45°, 60°, and 75° to determine how geometric sharpness affects aerodynamic performance. The study utilized Computational Fluid Dynamics (CFD) using the ANSYS Fluent solver. The Reynolds-Averaged Navier-Stokes (RANS) equations were solved using the Shear Stress Transport (SST) k-omega turbulence model, which is specifically suited for predicting flow separation under adverse pressure gradients. A Grid Independence Test was first performed to establish an optimal mesh resolution of 8 mm, ensuring numerical accuracy. The principal results demonstrated a significant correlation between the base angle and wake topology. The 45° prism exhibited a confined separation bubble and rapid flow recovery. In contrast, the 75° prism generated a massive recirculation zone with a severe velocity deficit, where the wake velocity dropped to 13 m/s, accompanied by the largest pressure differential between the front and rear faces. It is concluded that increasing the base angle significantly amplifies form drag by widening the wake and delaying pressure recovery. Consequently, shallower base angles are recommended for engineering applications requiring minimized aerodynamic resistance.

1. Introduction

The study of external fluid dynamics over bluff bodies is a cornerstone of aerodynamic and civil engineering, fundamental to the design of structures ranging from high-rise buildings to sensor housings and bridge decks [1]. Unlike streamlined bodies, where the flow remains attached to the surface, bluff bodies like triangular prisms are characterized by sharp corners that force the flow to separate [2]. This separation creates a complex wake region behind the object, dominated by

* *Corresponding author.*
E-mail address: dd220060@student.uthm.edu.my

https://doi.org/10.37934/afhme.8.1.3950a

recirculating eddies, low pressure, and significant aerodynamic drag [3]. Understanding these flow phenomena is essential for optimizing structural stability and predicting wind loads.

However, the flow behavior around a triangular prism is highly sensitive to its geometric orientation and shape, specifically the base angle. The abrupt change in geometry at the leading and trailing edges dictates the size of the recirculation zone and the intensity of the vortex shedding [4]. While the physics of simple cylinders and cubes are well-documented, the specific influence of varying base angles on the wake recovery and velocity deficit requires detailed investigation. Accurately predicting these phenomena has traditionally relied on costly wind tunnel experiments, but Computational Fluid Dynamics (CFD) has emerged as an indispensable and cost-effective tool for solving the governing equations over such complex geometries [5].

The primary aim of this study is to investigate the external flow dynamics around a triangular prism using ANSYS Fluent. This assignment critically evaluates how geometric variations influence aerodynamic performance. To achieve this, the study first establishes an optimal mesh through a Grid Independence Test (GIT) to ensure numerical accuracy. Subsequently, it simulates and compares the flow characteristics specifically velocity profiles, pressure distributions, and wake structures for three distinct base angles: 45°, 60°, and 75°. By analyzing these designs, the study aims to provide a quantitative understanding of how the prism geometry affects flow separation and aerodynamic drag.

2. Literature Review

2.1 Governing Equations and Turbulence Modelling

The flow of air around any object is mathematically described by the Navier-Stokes equations, which represent the conservation of mass and momentum [6]. For engineering applications where the flow is turbulent, directly solving these equations is too computationally expensive. Instead, the Reynolds-Averaged Navier-Stokes (RANS) equations are used. This method averages the flow fluctuations over time, introducing unknown terms called Reynolds stresses that must be solved using a turbulence model [7].

Choosing the right turbulence model is critical for accuracy. While the standard k-ε model is popular for general flows, it is often inaccurate for flows with strong separation, like those behind a prism [8]. In contrast, the Shear Stress Transport (SST) k-ω model is widely recommended for external aerodynamics because it better predicts the onset of flow separation and the size of the wake region [9].

2.2 Flow Separation and Wake Dynamics

A triangular prism is classified as a bluff body, meaning it is not streamlined. As fluid flows over the prism, the sharp corners force the flow to detach from the surface, a phenomenon known as flow separation [10]. This separation creates a shear layer that curls up behind the object to form a low-pressure recirculation zone or wake. The pressure difference between the front of the prism and the wake creates pressure drag, which is the dominant force on bluff bodies. The size and width of this wake are directly related to the amount of drag experienced by the object [11].

2.3 Effect of Prism Geometry

Research has shown that the wake structure is highly sensitive to the geometry of the object. For a triangular prism, the base angle dictates how abruptly the flow must change direction. Standard

fluid dynamics principles [12] indicate that varying the prism angle significantly alters the flow separation point while steeper angles typically result in wider wakes and higher drag coefficients due to the increased bluntness of the body. Understanding this relationship is crucial for practical applications, such as calculating wind loads on triangular building structures or bridge components.

3. Methodology

3.1 Geometry Development and Computational Domain

The geometry for this study was constructed using ANSYS DesignModeler. The primary object of interest is a triangular prism with a fixed base width of 0.2 m. To investigate the effect of aerodynamic shape on wake formation and drag, three distinct prism models were generated with varying base angles, θ of 45°, 60°, and 75°. These geometric configurations were specifically chosen to represent a range of bluff body sharpness, as illustrated in Figure 1.

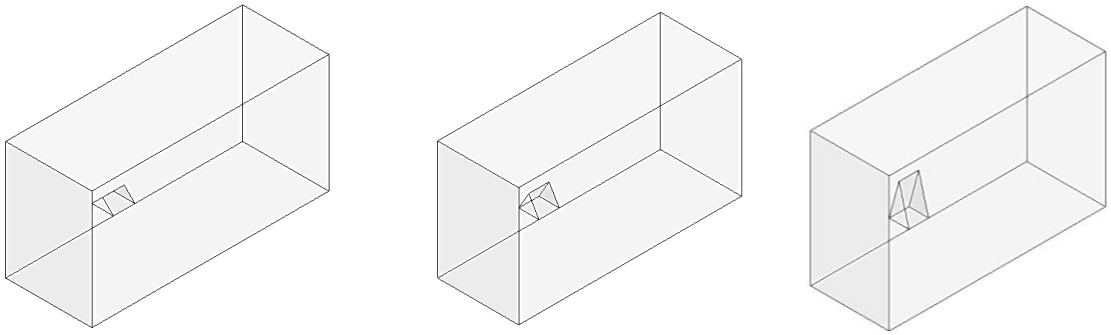

Fig. 1. Isometric view of the triangular prism geometries used for the simulation (a) 45° base angle (b) 60° base angle (c) 75° base angle

To simulate the external airflow around the prism, a computational fluid domain was created using the Enclosure operation. A non-uniform box cushion was applied surrounding the solid body, effectively representing the virtual wind tunnel. The dimensions of this enclosure were carefully selected to minimize boundary interference effects while ensuring computational efficiency. The domain extends 500 mm upstream from the prism to ensure a uniform approach flow, while the outlet boundary is extended significantly further, 1500 mm downstream, to allow for full wake development and to prevent reverse flow at the boundary [13].

In the transverse directions, the enclosure clearance was set to 300 mm in the spanwise direction and 500 mm in the vertical direction. These dimensions were chosen to ensure that the blockage ratio remains low, preventing the domain walls from artificially accelerating the flow or distorting the pressure field around the prism [14]. Finally, after generating the enclosure, a Boolean Subtract operation was automatically performed to remove the solid prism volume from the air domain, creating the hollow fluid cavity required for the CFD solver.

3.2 Mesh Generation

The discretization of the computational domain was performed using the ANSYS Meshing module. An unstructured mesh consisting primarily of tetrahedral elements was generated to accommodate the sharp corners of the triangular prism geometry. For the initial baseline simulation, a global element size of 50 mm was applied to the entire fluid domain. This relatively coarse

background mesh was sufficient for the far-field regions where flow gradients are low, ensuring computational efficiency by keeping the total node count manageable.

To accurately capture the complex flow physics near the prism walls and the immediate wake region, a localized refinement strategy was implemented using Face Sizing. While maintaining the global element size at 50 mm, the mesh resolution on the prism surfaces was progressively refined to conduct the Grid Independence Test (GIT). As detailed in the results, the face sizing was systematically reduced from 12 mm to 10 mm, 8 mm, and finally 6 mm. This approach ensured that the boundary layer separation and vortex shedding were resolved with increasing precision without unnecessarily increasing the cell count in the far-field [15].

3.3 Grid Independence Test (GIT)

The Grid Independence Test (GIT) is an essential verification step in all CFD simulations. Its purpose is to ensure that the numerical results are independent of the mesh resolution and that further mesh refinement does not lead to significant changes in the output. This validation step is vital to confirm the accuracy and stability of the simulation outcomes, particularly for external flows involving separation and wake formation.

A balance must be achieved between computational cost and solution accuracy. Coarse meshes like Test 1 may produce results with large discretization errors, while overly fine meshes increase computational time and memory usage without delivering proportional improvements in accuracy [16]. Therefore, an optimal mesh resolution is determined by evaluating the deviation in a key flow variable as the mesh is refined.

In this study, the GIT was conducted by evaluating the average wake velocity magnitude downstream of the triangular prism. The mesh was refined by progressively decreasing the Face Sizing on the prism surface, as detailed in the previous section. For each mesh, the velocity was recorded, and the percentage deviation between successive mesh configurations was computed using the formula shown in Eq. (1):

$$Deviation, \% = \frac{|\Delta V_{Mesh\ i+1} - \Delta V_{Mesh\ i}|}{\Delta V_{Mesh\ i+1}} \times 10 \quad (1)$$

where ΔV_i represents the velocity magnitude for the current mesh and ΔV_{i+1} represents the velocity magnitude for the next finer mesh.

3.4 Boundary Condition and Parameter Assumption

In this simulation, specific boundary conditions were applied to the computational domain to define the flow behaviour entering and exiting the virtual wind tunnel. These boundaries are illustrated in Figure 2, distinguishing between the flow inlet, the pressure outlet, and the solid wall surfaces. The inlet boundary was assigned a velocity-inlet condition with a uniform magnitude of 50 m/s flowing in the positive Z-direction. At the downstream boundary, a pressure-outlet condition of 0 Pa was imposed. This allows the fluid to exit the domain freely into the ambient atmosphere without artificial backflow.

The boundary conditions for the walls were treated distinctively. The surfaces of the triangular prism were assigned a no-slip wall condition, enforcing zero relative velocity between the air and the solid body. This is critical for accurately capturing the boundary layer development and the subsequent flow separation at the prism corners. Conversely, the outer walls of the enclosure which are top, bottom, and sides were set to Symmetry. This condition removes the shear stress at these boundaries, effectively simulating an open-air environment and preventing the outer walls from

interfering with the wake development [14]. For this study, the fluid was defined as air at standard atmospheric conditions. The density was set to 1.225 kg/m³ and the dynamic viscosity, μ to $1.7894 \times 10^{-5}\ kg/m \cdot s$, consistent with the International Standard Atmosphere (ISA) values [17].

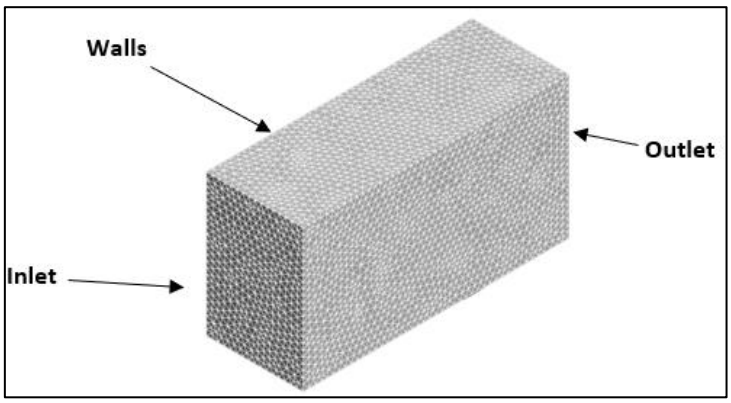

Fig. 2. Boundary zones applied to the computational domain

3.5 Numerical Setup

The numerical simulations were performed using the commercial CFD solver ANSYS Fluent. A pressure-based, steady-state solver was employed to solve the discretized governing equations. To close the Reynolds-Averaged Navier-Stokes (RANS) equations, the SST k-ω turbulence model was selected. This model blends the robust free-stream behaviour of the k-ε model with the accurate near-wall formulation of the k-ω model, making it superior for predicting flow separation under adverse pressure gradients [18].

The pressure-velocity coupling was handled using the Coupled algorithm. Unlike segregated schemes which solve the momentum and continuity equations sequentially, the Coupled scheme solves them simultaneously. This approach significantly improves the rate of convergence and robustness, particularly for steady-state flows involving strong acceleration around bluff bodies [19].

For spatial discretization, the Second-Order Upwind scheme was utilized for the momentum, turbulent kinetic energy, and specific dissipation rate equations. Unlike first-order schemes, which can introduce significant artificial viscosity, the second-order scheme minimizes numerical diffusion. This is critical for accurately resolving the sharp velocity gradients and vortex structures in the wake region behind the triangular prism [20]. The convergence criteria for all residuals were set to 1×10^{-4} to ensure a statistically steady solution.

4. Results and Discussion

4.1 Grid Independence Test (GIT) Verification Results

Before comparing the aerodynamic characteristics of the different prism angles, a Grid Independence Test (GIT) was conducted to select an optimal mesh. This step is crucial to ensuring that the simulation results are physically meaningful and not influenced by discretization errors. The average wake velocity magnitude was calculated for five progressively finer meshes, as summarized in Table 1. The mesh was refined by reducing the Face Sizing on the prism from 12 mm down to 6 mm, while keeping the global element size constant.

Figure 3 provides a visual comparison of the wake velocity profiles along the transverse direction for all five simulation cases. The graph clearly demonstrates the impact of mesh resolution on the flow prediction. The coarse mesh which is Test 1 acts as a significant outlier, predicting a much

shallower and wider wake deficit compared to the refined cases. This indicates that the default mesh was insufficient to resolve the strong shear layers and recirculation zone behind the prism.

Table 1
Grid independence test results

Simulation case	Element size (mm)	Body sizing (mm)	Number of elements	Number of nodes	Velocity magnitude (m/s)	Relative difference (%)
Test 1	50	-	73888	14686	39.6537	-
Test 2	50	12	125570	23828	37.8857	4.67
Test 3	50	10	145108	27377	37.5142	0.99
Test 4	50	8	177765	33276	37.7304	0.57
Test 5	50	6	248892	46189	37.5083	0.59

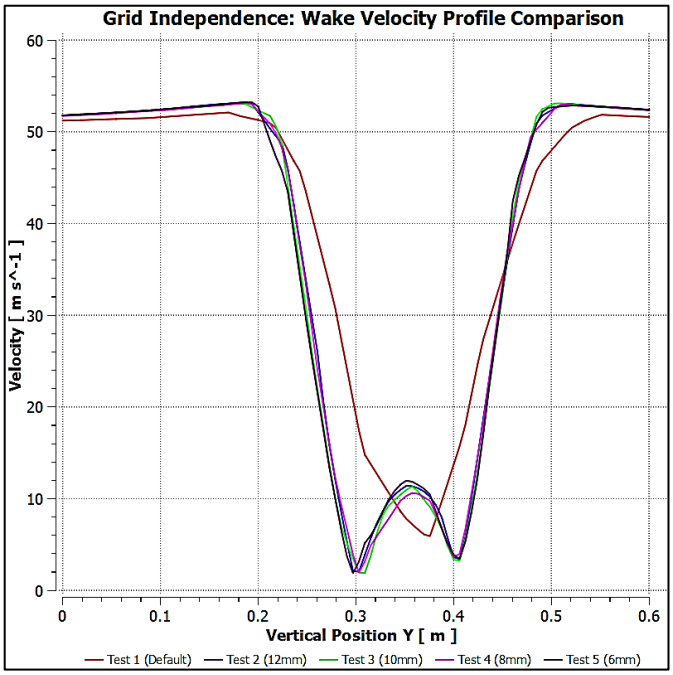

Fig. 3. Comparison of wake velocity profiles for varying mesh densities, demonstrating grid convergence

As the mesh resolution increased from Test 2 to Test 5, the velocity profiles began to converge onto a single solution. The deviation between Test 3 and Test 4 dropped to just 0.57%, indicating that the solution had stabilized. Further refinement to Test 5 resulted in a negligible change of -0.59%, proving that the results had achieved grid independence. Consequently, Test 4 was selected as the optimal mesh for this study. With 33,276 nodes, it provides a high degree of accuracy, virtually identical to the finest mesh while maintaining a lower computational cost than Test 5. This mesh setting was used for all subsequent simulations of the 45°, 60°, and 75° prisms.

4.2 Qualitative Flow Analysis

This section presents the qualitative results obtained from the CFD simulations. To thoroughly evaluate the flow physics around the triangular prisms, velocity magnitude contours were generated on the central symmetry plane. These visualizations provide a direct insight into the flow separation and wake formation mechanisms for the three different base angles.

4.2.1 Velocity distribution and wake structure

Figure 4 compares the velocity magnitude distribution for the 45°, 60°, and 75° prisms. In all three cases, the flow exhibits the characteristic behaviour of a bluff body: the flow accelerates around the sharp leading corners, indicated by the red and orange high-velocity zones, and separates to form a low-velocity wake region, shown in blue, downstream. However, the topology of this wake differs significantly between the geometries.

As shown in Figure 4(a), the 45° prism represents the most streamlined case among the three. The shallower base angle allows the shear layers to separate at a relatively narrow angle. Consequently, the resulting wake is confined, and the velocity deficit represented by the blue zone is the smallest of the three cases. The flow also appears to begin recovering momentum a short distance downstream, suggesting weaker vortex shedding and less flow disturbance.

In contrast, as the geometry becomes steeper, the aerodynamic obstruction becomes more severe. For the 60° prism in Figure 4(b), the wake region noticeably widens compared to the 45° case, indicating an expansion of the recirculation zone. The most dramatic effect, however, is observed in the 75° prism. The steep angle forces a massive flow separation, resulting in a wake that is significantly wider and extends much further downstream than in the other cases. The large, deep-blue region highlights a zone of very low velocity and high-pressure loss, confirming the theoretical expectation that steeper bluff bodies generate stronger turbulence and higher form drag.

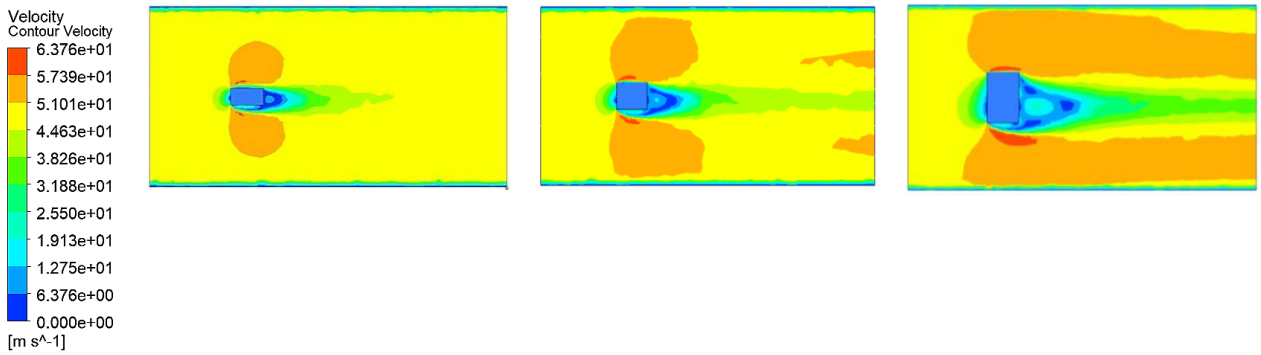

Fig. 4. Velocity magnitude contour on the symmetry plane (base angles) (a) 45° (b) 60° (c) 75°

4.2.2 Static pressure distribution analysis

The static pressure distribution around the triangular prisms provides critical insight into the aerodynamic forces acting on the body, particularly the form drags. Figure 5 illustrates the pressure contours for the three base angles. In all cases, the pressure field is characterized by a high-pressure stagnation region at the leading face where the flow impacts the body, and a low-pressure suction zone in the wake caused by flow separation.

Comparing the three geometries reveals a clear trend in how the base angle influences this pressure difference. For the 45° prism, the stagnation region at the leading edge is relatively concentrated. The corresponding low-pressure zone in the wake is also confined close to the rear surface, suggesting that pressure recovery begins earlier. This results in the smallest pressure differential between the front and rear faces. As the angle increases to 60°, the stagnation zone on the front face becomes noticeably wider due to the increased frontal area exposed to the flow. The low-pressure wake region also expands in size compared to the 45° case, indicating a stronger

separation bubble and a delay in pressure recovery. This intermediate state confirms that drag penalty increases progressively with the base angle.

Finally, the 75° prism exhibits the most intense aerodynamic resistance. It features a broad stagnation region on the windward face and a massive low-pressure wake that extends significantly downstream. The combination of high pressure at the front and a sustained low-pressure zone at the rear creates the largest pressure differential. This confirms that the 75° prism experiences the highest form drag among the three cases, consistent with the wake width observations in the previous section.

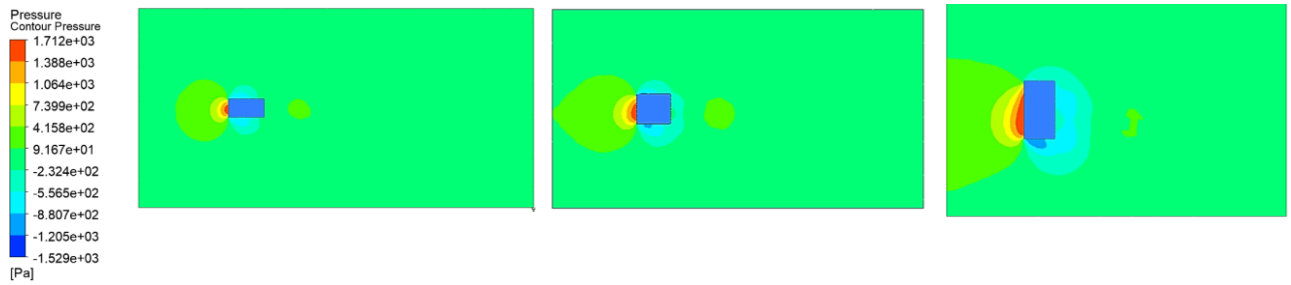

(a) (b) (c)

Fig. 5. Static pressure contour (base angles) (a) 45° (b) 60° (c) 75°

4.2.3 Streamline and recirculation zone analysis

To further investigate the flow topology, streamline visualizations were generated on the symmetry plane. Streamlines depict the path followed by instantaneous fluid particles, allowing for the clear identification of flow separation points, vortex formation, and the extent of the recirculation zone behind the bluff body. Figure 6 presents the streamline patterns for the three varying base angles.

In all three simulation cases, the streamlines confirm that the flow separates immediately at the sharp leading corners of the prism. The fluid cannot negotiate the abrupt change in geometry, causing it to detach and roll up into a pair of counter-rotating vortices immediately behind the rear face. However, the size and shape of these vortices differ dramatically depending on the prism angle.

For the 45°prism, the recirculation zone is relatively compact. The shear layers, the boundaries between the fast-moving free stream and the slow-moving wake, remain close to the body axis. The streamlines indicate that the flow attempts to reattach and straighten out a short distance downstream, resulting in a smaller wake "bubble."

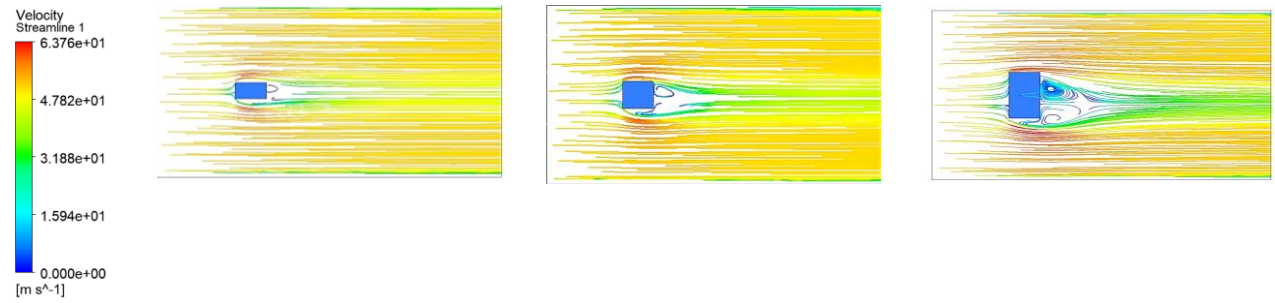

(a) (b) (c)

Fig. 6. Streamline visualization of the wake region (base angles) (a) 45° (b) 60° (c) 75°

As the base angle increases to 60° and finally 75°, the recirculation zone expands significantly. The steep 75° angle forces the flow to separate at a much wider angle, creating a massive region of

swirling, turbulent fluid. The streamlines in Figure 6(c) clearly show large, elongated vortices that occupy a significant volume behind the prism. This extended recirculation length effectively prevents the pressure from recovering, directly contributing to the high pressure drag observed in the previous section.

4.3 Quantitative Analysis of Wake Profiles

To quantify the aerodynamic differences observed in the contour plots, velocity profiles were extracted along transverse lines at three specific locations downstream of the prism trailing edge: Z = -0.1 m, Z = -0.4 m, and Z = -0.7 m. These plots allow for a direct numerical comparison of the wake width and the velocity deficit.

4.3.1 Near-wake characteristics, Z = -0.1m

Figure 7 illustrates the velocity profile immediately behind the prism. In this region, the flow is highly chaotic and dominated by the formation of shedding vortices. The 45° prism exhibits the narrowest wake profile. The velocity deficit is sharp but confined to a small transverse region, indicating a compact separation bubble. The 60° prism acts as an intermediate case, while its wake is wider than the 45° prism, it still maintains a relatively organized V-shape profile. In contrast, the 75° prism shows a dramatically wider velocity deficit. Furthermore, the profile shape for the 75° case is irregular, featuring multiple local minima. This structural complexity suggests the presence of a large, unstable twin-vortex system immediately behind the blunt trailing edge.

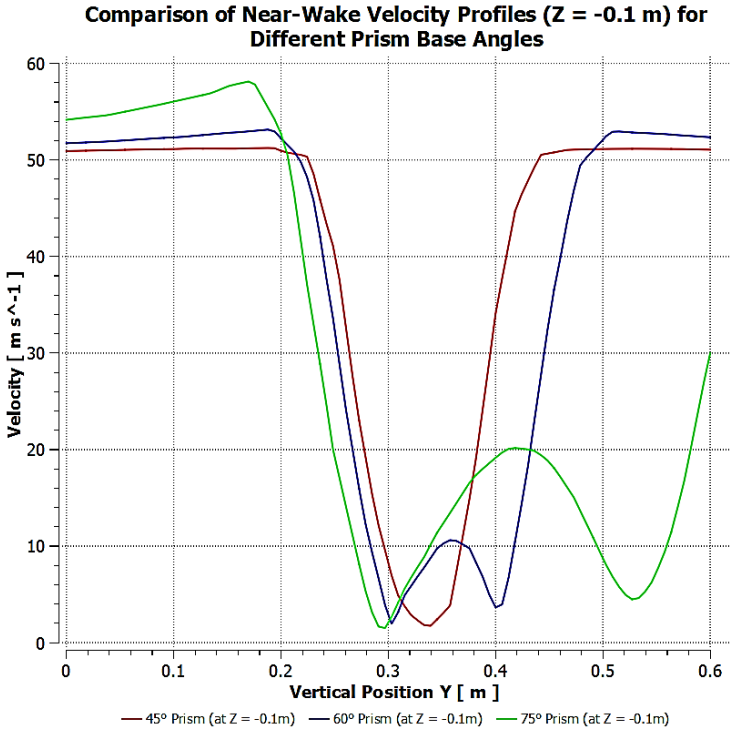

Fig. 7. Comparison of near-wake velocity profiles at Z = -0.1 m

4.3.2 Wake recovery and velocity deficit, Z = -0.4m

Moving further downstream to Z = -0.4 m, the differences in wake recovery become evident, as illustrated in Figure 8. The flow behind the 45° prism has already begun to recover significantly, with

the minimum velocity rising to approximately 38 m/s. The 60° prism follows a similar recovery trend but lags behind, with a minimum velocity of roughly 34 m/s. However, the 75° prism still exhibits a massive velocity deficit, with the speed dropping as low as 13 m/s. This huge difference quantitatively proves that the steepest prism generates a much stronger and more persistent drag force than the shallower angles.

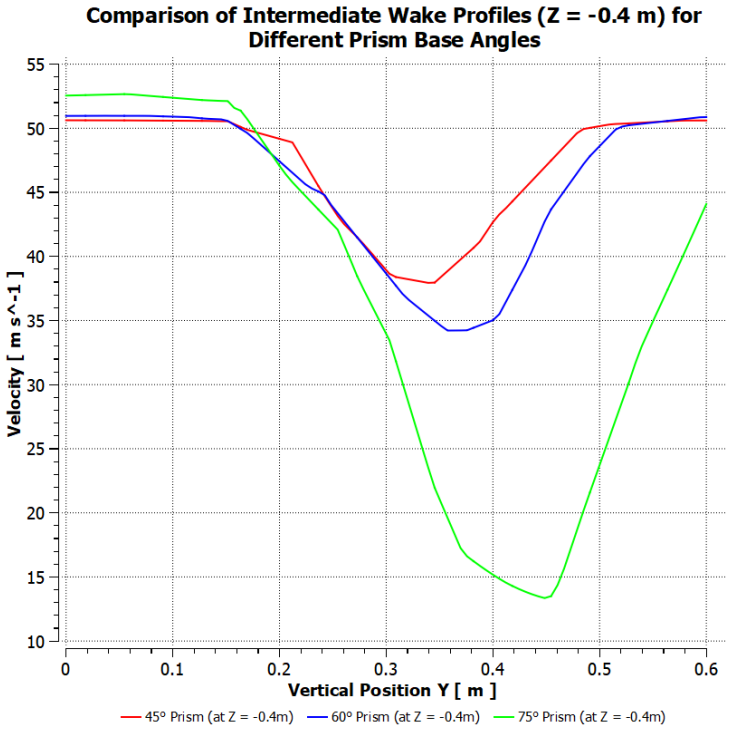

Fig. 8. Comparison of intermediate wake profiles at Z = -0.4 m

4.3.3 Far-field wake persistence, Z = -0.7m

In the far wake at Z = -0.7 m, the 45° and 60° profiles have largely returned to the free-stream velocity, leaving only a shallow depression, as illustrated in Figure 9. The 60° prism profile is now almost indistinguishable from the 45° case, indicating that its wake turbulence dissipates reasonably quickly. However, the 75° prism continues to disrupt the flow field significantly. Even at this distance, the wake velocity remains below 30 m/s, and the width of the disturbed region remains large. This persistence indicates that the large-scale turbulent structures generated by the steep 75° angle dissipate energy very slowly compared to the smaller eddies generated by the 45° and 60° prisms. This slow recovery is a hallmark of high-drag bluff bodies.

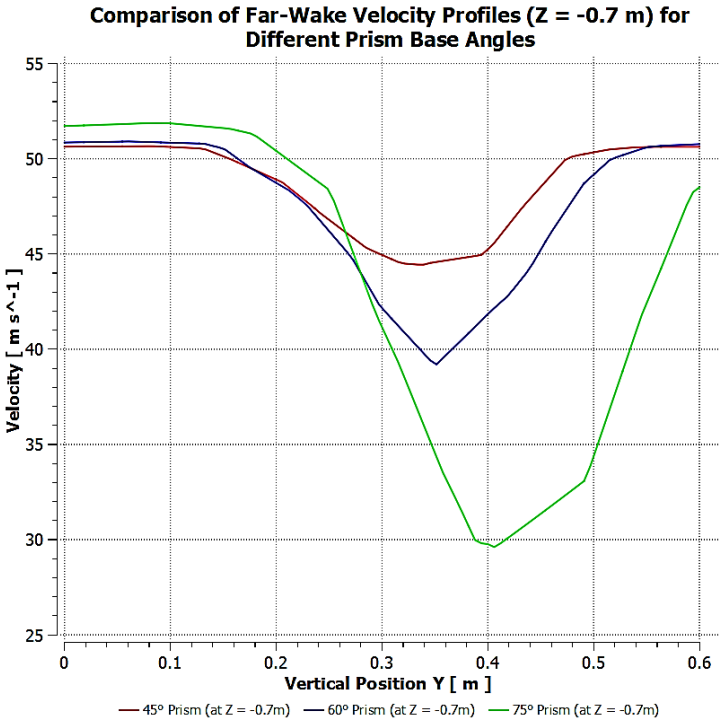

Fig. 9. Comparison of far-wake velocity profiles at Z = -0.7 m

5. Conclusions

This project successfully simulated the turbulent external flow over a triangular prism using ANSYS Fluent, achieving the primary objective of quantifying the effect of geometric variation on aerodynamic performance. The study first established a high-fidelity numerical setup by performing a GIT, identifying that an 8 mm Face Sizing mesh provided the optimal balance between numerical accuracy and computational cost. This rigorous validation step ensured that the subsequent flow analysis was physically meaningful and free from significant discretization errors.

The comparative analysis of the 45°, 60°, and 75° prisms revealed that the base angle is a critical determinant of both wake topology and aerodynamic drag. Qualitative results from velocity contours and streamlines demonstrated that increasing the base angle significantly widens the recirculation zone. The 45° prism exhibited a compact separation bubble with rapid flow reattachment, whereas the 75° prism generated a massive, turbulent wake that extended significantly downstream. This was further corroborated by the static pressure distributions, which confirmed that the steeper 75° angle created the most severe pressure differential between the windward stagnation face and the leeward suction face, resulting in the highest form drag among the three geometries.

Quantitatively, the extraction of velocity profiles proved that wake recovery is inversely related to the base angle. While the flow behind the 45° and 60° prisms recovered to near free-stream conditions by the far-field region, the 75° prism retained a massive velocity deficit, with near-wake velocities dropping as low as 13 m/s. This persistence indicates that the large-scale eddies generated by steeper bluff bodies dissipate energy much more slowly than the smaller structures found behind shallower angles. In conclusion, the study confirms that increasing the base angle of a triangular prism fundamentally alters the flow physics, transitioning the wake from a confined separation bubble to a wide, high-drag recirculation region, making shallower angles strictly preferable for applications requiring minimized wind resistance.

References

[1] Anderson, John. *EBOOK: Fundamentals of Aerodynamics (SI units)*. McGraw hill, 2011.
[2] White, Frank M. "Fluid mechanics, in SI units." (2012).
[3] Rodi, Wolfgang. *Turbulence models and their application in hydraulics*. Routledge, 2017. https://doi.org/10.1201/9780203734896
[4] Liu, Xu, Nan Gui, Hao Wu, Xingtuan Yang, Jiyuan Tu, and Shengyao Jiang. "Numerical simulation of flow past a triangular prism with fluid–structure interaction." *Engineering Applications of Computational Fluid Mechanics* 14, no. 1 (2020): 462-476. https://doi.org/10.1080/19942060.2020.1721332
[5] Versteeg, H. K., and W. Malalasekera. "Computational fluid dynamics: the finite volume method." *Harlow, England: Longman Scientific & Technical* (1995).
[6] Anderson, John D. *Computational fluid dynamics: the basics with applications*. New York: McGraw-Hill, 2002.
[7] Versteeg, Henk Kaarle. *An introduction to computational fluid dynamics the finite volume method, 2/E*. Pearson Education India, 2007.
[8] Rodi, Wolfgang. *Turbulence models and their application in hydraulics*. Routledge, 2017. https://doi.org/10.1201/9780203734896
[9] Menter, Florian R. "Two-equation eddy-viscosity turbulence models for engineering applications." *AIAA journal* 32, no. 8 (1994): 1598-1605. https://doi.org/10.2514/3.12149
[10] White, Frank M., and Joseph Majdalani. *Viscous fluid flow*. Vol. 3. New York: McGraw-Hill, 2006.
[11] Bearman, Peter W. "Vortex shedding from oscillating bluff bodies." *Annual Review of Fluid Mechanics* 16 (1984): 195-222. https://doi.org/10.1146/annurev.fl.16.010184.001211
[12] Çengel, Yunus A., Robert H. Turner, and R. Smith. "Fundamentals of thermal-fluid sciences." *Applied mechanics reviews* 54, no. 6 (2001): B110-B112. https://doi.org/10.1115/1.1421126
[13] Tu, Jiyuan, Guan Heng Yeoh, Chaoqun Liu, and Yao Tao. *Computational fluid dynamics: a practical approach*. Elsevier, 2023.
[14] Jensen, Andreas. "Recommendations on the Use of CFD in Wind Engineering." In *Cost action C*. 2004.
[15] Roache, Patrick J. "Perspective: a method for uniform reporting of grid refinement studies." (1994): 405-413. https://doi.org/10.1115/1.2910291
[16] Lee, Minhyung, Gwanyong Park, Changyoung Park, and Changmin Kim. "Improvement of grid independence test for computational fluid dynamics model of building based on grid resolution." *Advances in Civil Engineering* 2020, no. 1 (2020): 8827936. https://doi.org/10.1155/2020/8827936
[17] Atmosphere, Standard, and I. S. O. Standard. "2533: 1975." International Organization for Standardization, USA (May 1975) (1975).
[18] Menter, Florian R., Martin Kuntz, and Robin Langtry. "Ten years of industrial experience with the SST turbulence model." *Turbulence, heat and mass transfer* 4, no. 1 (2003): 625-632.
[19] Darwish, F. Moukalled L. Mangani M. *The Finite Volume Method in Computational Fluid Dynamics*. 2016. https://doi.org/10.1007/978-3-319-16874-6
[20] Barth, Timothy, and Dennis Jespersen. "The design and application of upwind schemes on unstructured meshes." In *27th Aerospace Sciences Meeting*, p. 366. 1989.. https://doi.org/10.2514/6.1989-366